Available online at www.sciencedirect.com
SCIENCE DIRECT®
ELSEVIER
European Journal of Mechanics B/Fluids 23 (2004) 279–302
EUROPEAN JOURNAL OF MECHANICS B/FLUIDS

Numerical study of flow around an inclined elliptic cylinder oscillating in line with an incident uniform flow

Serpil Kocabiyik [a,*], S.J.D. D'Alessio [b]

[a] *Department of Mathematics and Statistics, Memorial University of Newfoundland, St. John's, Newfoundland, A1C 5S7, Canada*
[b] *Department of Applied Mathematics, University of Waterloo, Waterloo, Ontario, N2L 3G1, Canada*

Received 13 December 2002; received in revised form 15 August 2003; accepted 2 September 2003

Abstract

Numerical calculations of the flow around an inclined elliptic cylinder oscillating in-line with the incident steady flow are reported at Reynolds number $R = 10^3$ and a fixed major–minor axis ratio of 0.5. The flow is incompressible and two-dimensional, and the in-line oscillations are harmonic. These oscillations are superimposed on the constant translational velocity as a single-frequency perturbation to examine the effect of increase of the perturbation amplitude and angle of inclination on the near-wake structure and the hydrodynamic forces acting on the cylinder. The numerical results lead to the postulation of two regimes for vortex shedding depending on the angle of inclination, which are discussed in some detail for exemplary cases.

Keywords: Unsteady; Incompressible; Viscous; Inline rectilinear oscillation; Elliptic cylinder

1. Introduction

The practical impetus for simulating the flow past cylindrical obstacles ranges from evaluation of the aerodynamic loading exerted on aerofoils to modelling the flow-induced vibrations of cylindrical elements of offshore structures exposed to waves. This paper presents the results of a numerical study of the unsteady flow generated by an infinitely long elliptic cylinder which is impulsively started into a uniform translational motion U combined with an oscillatory motion in-line with the horizontal direction of the translational motion. Specifically, the in-line oscillatory velocity has the form $U_m \cos \overline{\omega} t$ where t is the time, U_m is the maximum oscillatory velocity and $\overline{\omega} = 2\pi f$ with f the forced frequency of oscillation. Here we consider an ellipse, with major and minor axes $2a$ and $2b$, placed in a viscous incompressible fluid so that its major axis is inclined at an angle of incidence η to the horizontal direction in which the cylinder is oscillating and translating. The motion is assumed to be laminar and governed by the unsteady Navier–Stokes equations and the mass conservation equation. There are five dimensionless parameters characterizing the problem. These are: the Reynolds number $R = 2aU/\nu$ where ν is the coefficient of kinematic viscosity, the velocity ratio $\alpha = U_m/U$, the forcing Strouhal number $\Omega = a\overline{\omega}/U$, angle of inclination η and the minor-to-major axis ratio of the ellipse $r = b/a$.

Most of the previous theoretical and experimental studies relates to circular cylinders under recti-linear oscillations. A useful review of circular cylinder oscillations of this type is provided by Riley [1], Sarpkaya [2] (see also Sumer and Fredsøe [3]). For flows induced by an elliptic cylinder performing translational oscillations in the presence of an oncoming uniform stream references may be made only to the works of Okajima, Takata and Asanuma [4], and D'Alessio and Kocabiyik [5]. In both of these studies the problem of the flow past an elliptic cylinder which is forced to oscillate transversely to the oncoming uniform flow when the cylinder is positioned asymmetrically relative to the main flow was considered. The works of Davidson and

* Corresponding author.
E-mail address: serpil@math.mun.ca (S. Kocabiyik).

0997-7546/$ – see front matter
doi:10.1016/j.euromechflu.2003.09.001

Riley [6], Taneda [7], Hall [8], Badr and Kocabiyik [9] were concerned with the case of purely translational oscillations of an elliptic cylinder placed in a quiescent viscous fluid and translational oscillations were allowed only about an axis which coincides with either the major or minor axis of the ellipse except for Hall [8]. D'Alessio and Kocabiyik [5] have summarized the above mentioned works on elliptic cylinders performing translational oscillations.

There has been no work on the related case with which this paper is concerned, i.e., the case in which the inclined elliptic cylinder vibrates in-line with the horizontal free-stream direction. The method of solution adopted here is based on the use of truncated Fourier representations for the stream function and finite-difference method for solving the vorticity transport equation. The method was successfully used for unsteady uniform flow over a stationary inclined cylinder by Staniforth [10], and is also applicable to uniformly translating inclined elliptic cylinders under rotary and recti-linear oscillations (see, for example, D'Alessio, Dennis and Nguyen [11] and D'Alessio and Kocabiyik [5]). The essential purpose of the present paper is to examine the effects of the maximum oscillatory-to-translational velocity ratio and of the angle of inclination on the flow structure in the near-wake region as well as on the hydrodynamic forces acting on the cylinder for a fixed Reynolds number of $R = 10^3$, forcing Strouhal number of $\Omega = \pi$, and the minor-to-major axis ratio of $r = 0.5$. Calculations are made for moderate values of time for the cases: $\eta = \pi/4$ and $\alpha = 0.25,\ 0.5,\ 0.75$ and for $\eta = \pi/2$ and $\alpha = 0.25,\ 0.5$.

2. Formulation and method of solution

An elliptic cylinder whose axis coincides with the z-axis is placed in an unbounded cross-stream with approaching velocity U, and is positioned at an angle of inclination η relative to the x-axis so that the major and minor axes are along the axes of x and y, respectively. The cylinder is set in motion impulsively from rest at time $t = 0$ and is forced to perform harmonic oscillations in-line with the oncoming uniform flow. Unidirectional transverse oscillations of the cylinder are represented by the velocity $V(t) = U_m \cos\overline{\omega}t$. The physical model considered is shown in Fig. 1. In order to achieve a fixed grid with respect to the cylinder, it is necessary to use a non-inertial reference frame attached to the cylinder. Since the appropriate coordinates for the present problem are the elliptic coordinates (ξ, θ), we use the following transformation

$$x = \cosh(\xi + \xi_0)\cos\eta, \qquad y = \sinh(\xi + \xi_0)\sin\eta, \tag{1}$$

where the constant $\xi_0 = \tanh^{-1}(b/a)$ defines the surface of the cylinder. Using the elliptic coordinate system, with the origin at the center of the cylinder, the equations of motion can be written in terms of the vorticity (ζ) and the stream function (ψ) in dimensionless form as

$$\frac{\partial^2\psi}{\partial\xi^2} + \frac{\partial^2\psi}{\partial\theta^2} = M^2\zeta, \tag{2}$$

$$\frac{\partial\zeta}{\partial\tau} = \frac{1}{M^2}\left[\frac{2}{R}\left(\frac{\partial^2\zeta}{\partial\xi^2} + \frac{\partial^2\zeta}{\partial\theta^2}\right) + \left(\frac{\partial\psi}{\partial\theta}\frac{\partial\zeta}{\partial\xi} - \frac{\partial\psi}{\partial\xi}\frac{\partial\zeta}{\partial\theta}\right)\right]. \tag{3}$$

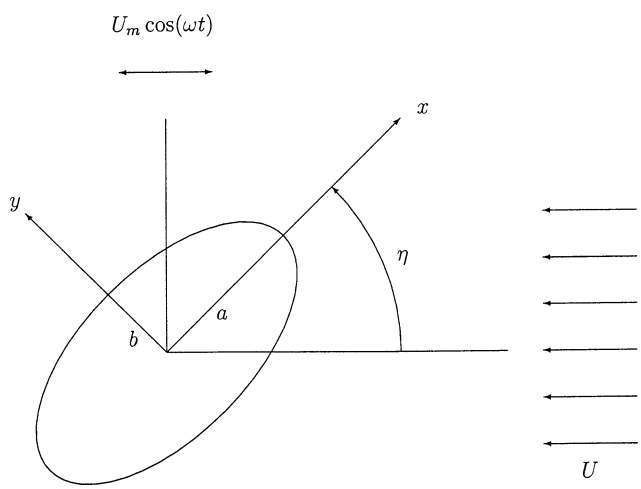

Fig. 1. Coordinate system and flow configuration.

The dependent variables ψ, ζ and τ in these equations are defined in terms of the usual dimensional quantities as $\psi^* = Ua\psi$, $\zeta^* = U\zeta/a$ and $t = a\tau/U$, and M^2 refers to the Jacobian of the transformation (1) is given by

$$M^2 = \frac{1}{2}\big[\cosh 2(\xi + \xi_0) - \cos 2\theta\big]. \tag{4}$$

The boundary conditions to be satisfied are the no-slip and impermeability conditions on the surface of ellipse:

$$\psi = \frac{\partial \psi}{\partial \xi} = 0 \quad \text{when } \xi = 0; \tag{5}$$

the periodicity conditions:

$$\psi(\xi, \theta + 2\pi, \tau) = \psi(\xi, \theta, \tau), \qquad \zeta(\xi, \theta + 2\pi, \tau) = \zeta(\xi, \theta, \tau); \tag{6}$$

and the free-stream conditions far away from the cylinder:

$$\frac{\partial \psi}{\partial \xi} \to \frac{1}{2}\,\mathrm{e}^{\xi+\xi_0}\big[\sin(\theta + \eta) + \alpha\cos(\Omega\tau)\sin(\theta + \eta)\big] \quad \text{as } \xi \to \infty, \tag{7a}$$

$$\frac{\partial \psi}{\partial \theta} \to \frac{1}{2}\,\mathrm{e}^{\xi+\xi_0}\big[\cos(\theta + \eta) + \alpha\cos(\Omega\tau)\cos(\theta + \eta)\big] \quad \text{as } \xi \to \infty, \tag{7b}$$

$$\zeta \to 0 \quad \text{as } \xi \to \infty. \tag{7c}$$

There is no explicit boundary condition for the vorticity on the cylinder surface. The surface vorticity can be computed from the known stream function distribution near the surface using (2); however, the large velocity gradient near the surface presents a numerical obstacle to such computations. Alternatively, in this study, integral conditions are used to predict the surface vorticity accurately. Detailed derivations of equations and boundary conditions similar to the ones used in this study are given in the recent work of D'Alessio and Kocabiyik [5] for the case an inclined elliptic cylinder under recti-linear oscillations in a transverse direction to that of the uniform free-stream. This section briefly summarizes the equations and the boundary conditions.

It may be shown that the conditions (5) and (7) can be combined, after integrating (2), to give another set of conditions of global type, namely

$$\int_0^\infty \int_0^{2\pi} M^2 \zeta(\xi, \theta, \tau)\,\mathrm{d}\theta\,\mathrm{d}\xi = 0, \tag{8a}$$

$$\int_0^\infty \int_0^{2\pi} \mathrm{e}^{-n\xi} M^2 \zeta(\xi, \theta, \tau)\cos(n\theta)\,\mathrm{d}\theta\,\mathrm{d}\xi = \pi\,\mathrm{e}^{\xi_0}\big[\sin\eta + \alpha\cos(\Omega\tau)\sin\eta\big]\delta_{1,n}, \tag{8b}$$

$$\int_0^\infty \int_0^{2\pi} \mathrm{e}^{-n\xi} M^2 \zeta(\xi, \theta, \tau)\sin(n\theta)\,\mathrm{d}\theta\,\mathrm{d}\xi = \pi\,\mathrm{e}^{\xi_0}\big[\cos\eta + \alpha\cos(\Omega\tau)\cos\eta\big]\delta_{1,n}, \tag{8c}$$

for all integers $n \geqslant 1$ with $\delta_{m,n}$ denoting the Kronecker delta function defined by

$$\delta_{m,n} = 1 \quad \text{if } m = n, \qquad \delta_{m,n} = 0 \quad \text{if } m \neq n.$$

These are employed in the solution procedure to ensure that all necessary conditions of the problem are satisfied. It is noted that the satisfaction of (8a) is necessary in order for the pressure to remain a periodic function of θ. These conditions also give constraints on the vorticity and can be used instead of the gradient conditions (7a,b) to calculate the surface vorticity. They are, in fact, equivalent to the one-dimensional form of the Green theorem constraint given by Dennis and Quartapelle [12]. The method of solution is an extension of the method developed by Staniforth [10] that takes into account cylinder oscillations that are in-line with the horizontal direction of the uniform free-stream. In a recent work by D'Alessio and Kocabiyik [5] the numerical technique of Staniforth was successfully modified to compute the flow around an inclined elliptic cylinder subjected to transverse oscillations whereby the stream function was expressed in the form of a Fourier series

$$\Psi(\xi, \theta, \tau) = \frac{1}{2}F_0(\xi, \tau) + \sum_{n=1}^{\infty}\big(F_n(\xi, \tau)\cos n\theta + f_n(\xi, \tau)\sin n\theta\big). \tag{9}$$

Because of the impulsive start, this gives rise to a singularity in the vorticity at $\tau = 0$. Thus, it is impossible to represent the vorticity ζ at $\tau = 0$ as required by a numerical scheme. Further, for small τ, the vorticity cannot be accurately represented by a finite-difference scheme. To overcome these difficulties, we make the following boundary-layer type transformation

$$\xi = kz, \quad k = 2(2\tau/R)^{1/2}; \quad \psi = k\Psi, \quad \zeta = \omega/k, \tag{10}$$

which maps the initial flow onto the scale of the boundary-layer thickness and removes the singularity in the vorticity at $\tau = 0$ due to the impulsive start. All the appropriate equations must be rescaled accordingly; for example,

$$F_n = kF_n^*, \qquad f_n = kf_n^*.$$

The equations and boundary conditions at the cylinder surface satisfied by the functions f_n^*, F_n^* are given by D'Alessio and Kocabiyik [5] and the far field conditions in the present case take the form (suppressing all stars)

$$\mathrm{e}^{-kz} F_0 \to 0, \qquad \mathrm{e}^{-kz} \frac{\partial F_0}{\partial z} \to 0, \tag{11a}$$

$$\mathrm{e}^{-kz} F_n \to \frac{1}{2k} \mathrm{e}^{\xi_0} \big[\sin\eta + \alpha \cos(\Omega\tau) \sin\eta\big] \delta_{n,1}, \quad \mathrm{e}^{-kz} \frac{\partial F_n}{\partial z} \to \frac{1}{2} \mathrm{e}^{\xi_0} \big[\sin\eta + \alpha \sin(\Omega\tau) \sin\eta\big] \delta_{n,1}, \tag{11b}$$

$$\mathrm{e}^{-kz} f_n \to \frac{1}{2k} \mathrm{e}^{\xi_0} \big[\cos\eta + \alpha \cos(\Omega\tau) \cos\eta\big] \delta_{n,1}, \qquad \mathrm{e}^{-kz} \frac{\partial f_n}{\partial z} \to \frac{1}{2} \mathrm{e}^{\xi_0} \big[\cos\eta + \alpha \cos(\Omega\tau) \cos\eta\big] \delta_{n,1}, \tag{11c}$$

for $n = 1, 2, \ldots$. It is noted that the far-field conditions given by (11b,c) differ from those given in D'Alessio and Kocabiyik owing to the difference in cylinder motions.

To initiate the integration procedure, the initial solution, obtained following the work by D'Alessio and Kocabiyik, at $t = 0$ is used. This initial solution forms the starting point of the numerical integration procedure and is given by

$$\omega_0(z, \theta, 0) = \frac{2}{\sqrt{\pi}} \frac{\mathrm{e}^{\xi_0}}{M_0} \big[\sin(\theta + \eta) + \alpha \sin(\theta + \eta)\big] \mathrm{e}^{-M_0^2 z^2}, \tag{12a}$$

$$F_0(z, 0) = 0, \quad F_n(z, 0) = \frac{\mathrm{e}^{\xi_0}}{M_0} [\sin\eta + \alpha \sin\eta] \left[M_0 z \operatorname{erf}(M_0 z) - \frac{1}{\sqrt{\pi}} \big(1 - \mathrm{e}^{-M_0^2 z^2}\big) \right] \delta_{n,1}, \tag{12b}$$

$$f_n(z, 0) = \frac{\mathrm{e}^{\xi_0}}{M_0} [\cos\eta + \alpha \cos\eta] \left[M_0 z \operatorname{erf}(M_0 z) - \frac{1}{\sqrt{\pi}} \big(1 - \mathrm{e}^{-M_0^2 z^2}\big) \right] \delta_{n,1}. \tag{12c}$$

Here $\operatorname{erf}(M_0 z)$ denotes the error function and $M_0^2 = [\cosh 2\xi_0 - \cos 2\theta]/2$.

3. Numerical integration procedure

The numerical method implemented to calculate the flow for finite but sufficiently high Reynolds number and moderate values of the time, is similar to the numerical method of integration given by D'Alessio and Kocabiyik [5] and is described below. The solutions of the transformed Navier–Stokes equations in terms of the boundary-layer coordinates (z, θ) for the scaled vorticity, ω, is approximated using a scheme similar to the Crank–Nicolson implicit procedure to advance the solution step-by-step in time. At a time τ the equation for the scaled vorticity can be written in the form

$$\tau \frac{\partial \omega}{\partial \tau} = q(z, \theta, \tau), \tag{13}$$

where

$$q(z, \theta, \tau) = \frac{1}{4M_z^2} \frac{\partial^2 \omega}{\partial z^2} + \frac{z}{2} \frac{\partial \omega}{\partial z} + \frac{\omega}{2} + \frac{k^2}{4M_z^2} \frac{\partial^2 \omega}{\partial \theta^2} + \frac{\tau}{M_z^2} \left(\frac{\partial \Psi}{\partial \theta} \frac{\partial \omega}{\partial z} - \frac{\partial \Psi}{\partial z} \frac{\partial \omega}{\partial \theta} \right). \tag{14}$$

The Crank–Nicolson finite difference approximation of Eq. (13) advances the known solution at time τ to time $\tau + \Delta\tau$ and is given by

$$\frac{1}{\Delta\tau} \big[\omega(z, \theta, \tau + \Delta\tau) - \omega(z, \theta, \tau)\big] = \frac{1}{2} \big[q(z, \theta, \tau + \Delta\tau) + q(z, \theta, \tau)\big], \tag{15}$$

where $\Delta\tau$ is the time increment. Since $q(z, t)$ depends on $\omega(z, t)$ and its derivatives the scheme is implicit. It is noted that explicit methods of solution of the vorticity transport equation is computationally expensive since an extremely small time

increment $\Delta\tau$ is necessary to achieve numerical stability. The boundary conditions used in solving the vorticity transport equation include both the periodicity condition and the far-field conditions given by

$$\omega(z,\theta,\tau)=\omega(z,\theta+2\pi,\tau) \quad \text{and} \quad \omega(z_\infty,\theta,\tau)=0, \tag{16a,b}$$

respectively. Since the problem is solved numerically, the condition at infinity (16b) is applied along $z=z_m$ where z_m denotes the outer boundary approximating infinity. Applying Eq. (15) at every mesh point in the range $0<z<z_m$ results in a nonlinear system of algebraic equations which is solved iteratively using the Gauss–Seidel procedure, after approximating all spatial derivatives in (14) using central differences. The boundary condition for the surface vorticity $\omega(0,\theta,\tau)$, which is needed to complete the integration procedure, is found to be

$$\omega(0,\theta,\tau)=\frac{1}{\pi M_0^2}\int_0^{2\pi}\left\{\frac{1}{2}\left(M_z^2\omega\right)\big|_{z=0}+\sum_{n=1}^{\infty}\left[\left(M_z^2\omega\right)\big|_{z=0}\sin n\theta+\left(M_z^2\omega\right)\big|_{z=0}\cos n\theta\right]\right\}\mathrm{d}\theta. \tag{17}$$

Equations for the Fourier components $f_n(z,\tau)$ and $F_n(z,\tau)$ of the scaled stream function at a fixed value of τ are of the form

$$g_n''-\beta^2 g_n=r_n(z,\tau), \tag{18}$$

where $\beta=nk$ and the prime refers to differentiation with respect to z. A straightforward finite difference solution for this equation may result in an unstable solution especially for large β. The method of solving these equations accurately is a specialized method dependent on the parameter β and is very closely linked to the satisfaction of the integral conditions (8). We shall give a description of the basis of this procedure here. This was not explained in detail by D'Alessio and Kocabiyik [5]. Eq. (18) can be split into two first order equations by introducing the functions P_n and Q_n such that

$$P_n=\frac{\partial f_n}{\partial z}-\beta f_n, \qquad Q_n=\frac{\partial f_n}{\partial z}+\beta f_n. \tag{19a,b}$$

Then,

$$\frac{\partial P_n}{\partial z}+\beta P_n=r_n, \qquad \frac{\partial Q_n}{\partial z}-\beta Q_n=r_n, \tag{20a,b}$$

and consequently

$$f_n=\frac{Q_n-P_n}{2\beta}, \qquad {f_n}'=\frac{Q_n+P_n}{2} \tag{21}$$

with

$$P_n=Q_n=\frac{\partial P_n}{\partial z}=\frac{\partial Q_n}{\partial z}=0 \tag{22}$$

on the cylinder surface. The first of Eqs. (20) can be integrated in the direction of increasing z to obtain

$$P_n(z+h,\tau)=\gamma P_n(z,\tau)+\gamma\,\mathrm{e}^{-\beta z}\int_z^{z+h}\mathrm{e}^{\beta\xi}r_n(\xi,\tau)\,\mathrm{d}\xi, \tag{23}$$

where $\gamma=\mathrm{e}^{-\beta h}$. A very simple step-by-step formula is obtained by assuming $r_n(z,\tau)$ to be constant in $z\leqslant\xi\leqslant z+h$ and equal to its value at $\xi=z$, for example. This gives

$$P_n(z+h,\tau)=\gamma P_n(z,\tau)+(1-\gamma)r_n(z,\tau)/\beta, \tag{24}$$

which is stable since $\gamma<1$.

More accurate formulae can be obtained by using other methods of evaluating the integral in (23). For example, we can approximate $r_n(z,\tau)$ by a linear function of z on the interval z to $z+h$ and evaluate the integral in (23) by parts where h is the step size in z-direction. An even more accurate formula on the interval z to $z+2h$ can be found by approximating $r_n(z,\tau)$ by a quadratic over the three grid points on the interval. This method, known as Filon integration, yields the result

$$\begin{aligned}P_n(z+2h,\tau)=\gamma^2P_n(x,\tau)&+\left[\frac{1-\gamma^2}{h^2\beta^3}+\frac{3\gamma^2-1}{2h\beta^2}-\frac{\gamma^2}{\beta}\right]r_n(x,t)-2\left[\frac{1-\gamma^2}{h^2\beta^3}-\frac{1+\gamma^2}{h\beta^2}\right]r_n(x+h,t)\\&+\left[\frac{1-\gamma^2}{h^2\beta^3}-\frac{\gamma^2+3}{2h\beta^2}+\frac{1}{\beta}\right]r_n(z+2h,\tau).\end{aligned} \tag{25}$$

Eq. (24) can be improved for the first interval $z = 0$ to $z = h$ by using a parabolic approximation to $r_n(z, \tau)$ and fitting it to the three points at $z = 0,\ h,\ 2h$. Thus we calculate $P_n(h, \tau)$ from

$$P_n(h,\tau) = \gamma P_n(0,\tau) + \left[\frac{1-\gamma}{h^2\beta^3} + \frac{1-3\gamma}{2h\beta^2} - \frac{\gamma}{\beta}\right] r_n(0,\tau) - \left[\frac{2(1-\gamma)}{h^2\beta^3} - \frac{2\gamma}{h\beta^2} - \frac{1}{\beta}\right] r_n(h,\tau) + \left[\frac{1-\gamma}{h^2\beta^3} - \frac{1+\gamma}{2h\beta^2}\right] r_n(2h,\tau). \tag{26}$$

Hence from a given approximation to $r_n(z, \tau)$ at a given time we can generate a solution for P_n using first (26) and then (25), step-by-step. If we follow the same procedure with (20b) for Q_n the method is highly unstable with an exponential error growth. However, the integration backwards from $z = z_m$ is stable provided that we can specify a condition for Q_n at $z = z_m$. To do this we assume that z_m is large enough that the uniform stream conditions relative to the cylinder are established and that the flow at $z = z_m$ is unaffected by transport of vorticity from the regions nearer to the cylinder. This is in any case implied in the assumptions (16b). Under these assumptions at time τ we then have that

$$Q_n(z_m,\tau) = 2\delta_{n,1}\,\mathrm{e}^{z_m\beta}. \tag{27}$$

In performing this backward integration we must ensure that when the boundary $z = 0$ is reached the function $Q_n(z, \tau)$ shall become zero. The function Q_n satisfies

$$\frac{\partial}{\partial z}\left(Q_n \mathrm{e}^{-\beta z}\right) = \mathrm{e}^{-\beta z} r_n, \tag{28}$$

and hence integrating from $z = 0$ to $z = z_m$ we obtain, using the result (27),

$$-Q_n(0,\tau) + 2\delta_{n,1} = \int_0^{z_m} \mathrm{e}^{-\beta z} r_n(z,\tau)\,\mathrm{d}z. \tag{29}$$

Hence if the conditions (8) are satisfied with the upper limit in the integral replaced by z_m, it follows from (29) that $Q_n(0, \tau) = 0$, as required. The backward step-by-step formula obtained from (20b) is given by

$$Q_n(z,\tau) = \gamma Q_n(z+h,\tau) - \mathrm{e}^{\beta z}\int_z^{z+h} \mathrm{e}^{-\beta\xi} r_n(\xi,\tau)\,\mathrm{d}\xi, \tag{30}$$

and we can easily obtain backward integration formulae corresponding to (25) and (26) by simple modifications to those formulae. The formula corresponding to (26) serves to calculate $Q_n(z_m - h, t)$ and then that corresponding to (25) continues the backward integrations. A discussion of the numerical stability of the method has been given in Dennis and Chang [13]. The main point in the use of these special methods when $\beta \neq 0$ is that the solution of (18) can be obtained when β is reasonably large using the same grid size h.

The whole iterative numerical scheme can be summarized as follows.

1. At time $\tau + \Delta\tau$, the known solution (12) at time τ ($\equiv 0$) is used as initial data. The matrix system resulting from (15) is solved using the most recently available information to obtain the functions $\omega(z, \theta, \tau + \Delta\tau)$.
2. Apply the integral conditions (8) to obtain a better approximation for $\omega(0, \theta, \tau + \Delta\tau)$.
3. Solve equation of the form (18) using the stable step-by-step numerical procedure mentioned above to obtain $f_n(z, \tau + \Delta\tau)$ and $F_n(z, \tau + \Delta\tau)$.
4. Repeat steps 1, 2 and 3 until convergence is reached. The condition set for convergence is $|\omega^{(m+1)}(z, \theta, \tau + \Delta\tau) - \omega^{(m)}(z, \theta, \tau + \Delta\tau)| < 10^{-5}$, where m denotes the iteration number.
5. Increment time and return to step 1.

It may also be necessary to subject the surface vorticity to under-relaxation in order to obtain convergence. Following the start of fluid motion, very small time steps ($\Delta\tau = 10^{-5}$) are taken since the time variation of the vorticity field is quite fast due to the impulsive start. However, as time increases the time step is gradually increased until reaching $\Delta\tau = 0.01$. The grid size Δz in the coordinate z, defined by $\xi = 2(2t/R)^{1/2}z$, is more or less independent of R. The number of points in the z-direction is taken as 201 with a space step of $\Delta z = 0.06$. This makes $z_\infty = 12$ which sets the outer boundary at a physical distance of about 40 major axis lengths away for a Reynolds number $R = 10^3$ and time $\tau = 12$. Thus the boundary is sufficiently far away so that the application of the boundary conditions (11a)–(11c) does not affect the solution in the viscous region near the cylinder surface. The maximum number of terms retained in the series (9) was 51 which corresponds to an upper limit of

$N = 25$ in the sums. Checks are made for $R = 10^3$ at several typical values of τ to ensure that N is large enough. This is done by increasing N and observing that the solution did not change appreciably. The computational parameters are to some extent chosen to be comparable with those used by D'Alessio and Kocabiyik [5], since these were found to be satisfactory and were checked carefully. Moreover, this scheme is tested against the results of Staniforth [10] for the non-oscillating (i.e., purely translating) case using similar Reynolds numbers; tests indicate that solutions are quite accurate. Finally, we note that the numerical method described may be used to continue the solution for increasing τ in terms of the physical coordinate ξ when the boundary layer thickens. However, in the present paper, only the case of $R = 10^3$ is presented, and it is possible to work in terms of the boundary-layer coordinate z over the entire range of τ considered.

4. Results

If L and D are the lift and drag on the cylinder, the total drag, C_D, and total lift, C_L, coefficients are defined by $C_D = D/\rho U^2 a$ and $C_L = L/\rho U^2 a$, respectively. The drag and lift coefficients can be obtained from

$$C_D = \left[\frac{2\sinh\xi_0}{R}\int_0^{2\pi}\left(\frac{\partial\zeta}{\partial\xi}\right)_{\xi=0}\sin\theta\,\mathrm{d}\theta - \frac{2\cosh\xi_0}{R}\int_0^{2\pi}(\zeta)_{\xi=0}\sin\theta\,\mathrm{d}\theta\right]\cos\eta + \left[\frac{2\cosh\xi_0}{R}\int_0^{2\pi}\left(\frac{\partial\zeta}{\partial\xi}\right)_{\xi=0}\cos\theta\,\mathrm{d}\theta - \frac{2\sinh\xi_0}{R}\int_0^{2\pi}(\zeta)_{\xi=0}\cos\theta\,\mathrm{d}\theta\right]\sin\eta - \pi\alpha\Omega\sin(\Omega\tau)\cosh\xi_0\sinh\xi_0, \tag{31}$$

$$C_L = \left[\frac{2\sinh\xi_0}{R}\int_0^{2\pi}\left(\frac{\partial\zeta}{\partial\xi}\right)_{\xi=0}\sin\theta\,\mathrm{d}\theta - \frac{2\cosh\xi_0}{R}\int_0^{2\pi}(\zeta)_{\xi=0}\sin\theta\,\mathrm{d}\theta\right]\sin\eta + \left[-\frac{2\cosh\xi_0}{R}\int_0^{2\pi}\left(\frac{\partial\zeta}{\partial\xi}\right)_{\xi=0}\cos\theta\,\mathrm{d}\theta + \frac{2\sinh\xi_0}{R}\int_0^{2\pi}(\zeta)_{\xi=0}\cos\theta\,\mathrm{d}\theta\right]\cos\eta, \tag{32}$$

where the first and the third integrals in each gives the coefficient due to the pressure and the second and the fourth that due to friction. We note that the fifth term of C_D is the inviscid drag coefficient due to the accelerating imposed flow which would have been exerted on the fluid displaced by the cylinder.

The numerical results are grouped in three cases (i) $\eta = \pi/4$, (ii) $\eta = \pi/6, \pi/3$, (iii) $\eta = \pi/2$ with $R = 10^3$, $\Omega = \pi$ and $r = 0.5$ to investigate effects of angle of inclination η and of the velocity ratio α, respectively. In the case of $\eta = \pi/4$ the problem is solved for three values of the velocity ratio, $\alpha = 0.25, 0.5, 0.75$. The case of $\eta = \pi/2$ the problem is investigated for $\alpha = 0.25, 0.5$. On the other hand, in the cases of $\eta = \pi/6,\ \pi/3$ the calculations are carried out only for the case when $\alpha = 0.5$. The results are presented in the form of streamline patterns as well as the variations of the drag and lift coefficients with time. In all streamline plots to be presented the oncoming flow is from right to left.

4.1. Streamline patterns for $R = 10^3$, $\Omega = \pi$ and $r = 0.5$ when $0.25 \leqslant \alpha \leqslant 0.75$

To discuss the effect of the angle of inclination on the vortex patterns the flow is calculated with $\eta = \pi/6, \pi/4, \pi/3, \pi/2$ when $0.25 \leqslant \alpha \leqslant 0.75$. Since all cases considered have $f = 0.5$ or $T \equiv 1/f = 2$ as the period of cylinder oscillation, a complete cycle consists of the following four stages: at $\tau = 0$ the ellipse starts to oscillate with its maximum velocity to the right and at $\tau = 0.5$ the ellipse reaches its maximum horizontal displacement in the positive horizontal direction and is in an instantaneous state of rest; at $\tau = 1$ the ellipse is in its equilibrium position and attains maximum velocity to the left; at $\tau = 1.5$ the ellipse is at its maximum horizontal displacement in the negative horizontal direction and is again in an instantaneous state of rest; and finally at $\tau = 2$ the ellipse is in its starting position and this pattern repeats itself. At the forced frequency of oscillation $f = 0.5$ considered in this study, synchronized vortex modes become locked to the cylinder oscillations which are higher than the otherwise natural Kármán vortex shedding frequency.

Streamline patterns are portrayed in Fig. 2 for the case of $\eta = \pi/6$ when $\alpha = 0.5$. Vortex shedding is initiated from the left side of the cylinder during the first quarter of the oscillation cycle after the start of the fluid motion and two opposite-sign vortices are shed in the first half-cycle of oscillation. After a while this vortex pair detaches and moves downstream initiating the alternate vortex shedding process. Figs. 2(a)–(e) show five snapshots of the flow at instants in time during the sixth cycle of oscillation for the time interval $10.0 \leqslant \tau \leqslant 12.0$. Close to the cylinder, Fig. 2(b), two adjacent vortex pairs of the same sign exist in the upper half of the cylinder and are shed away to form a double co-rotating vortex pair at time $\tau = 11$. Moreover,

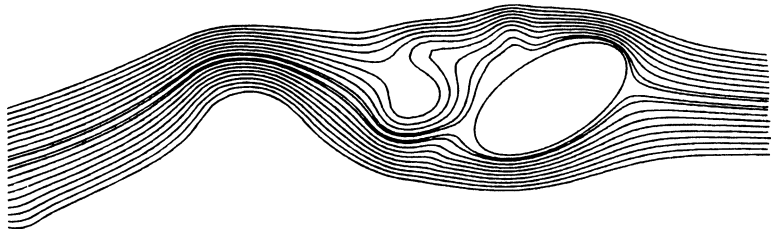

(a)

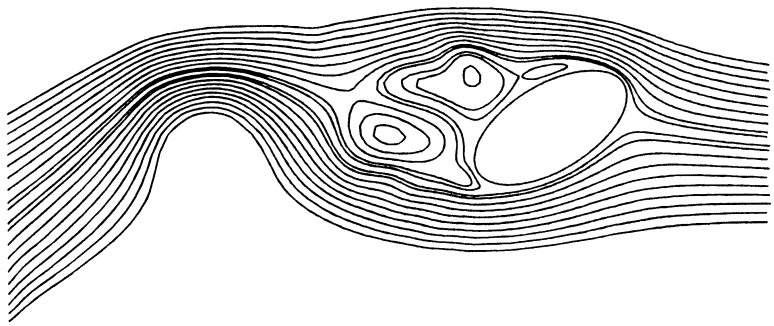

(b)

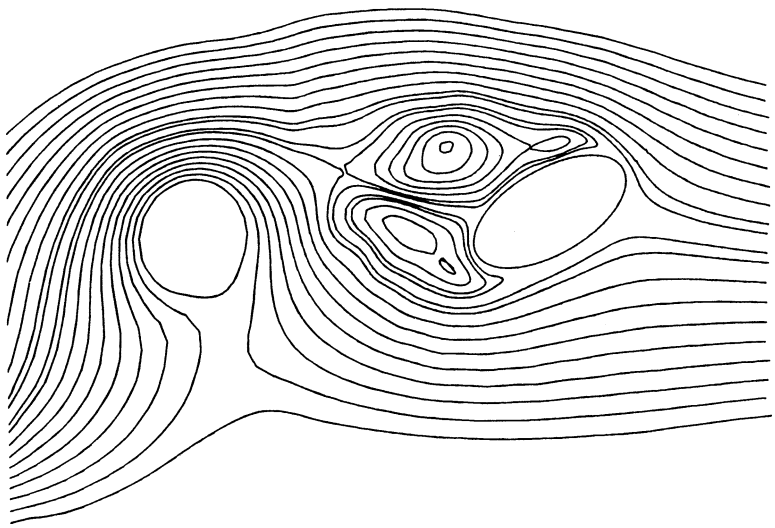

(c)

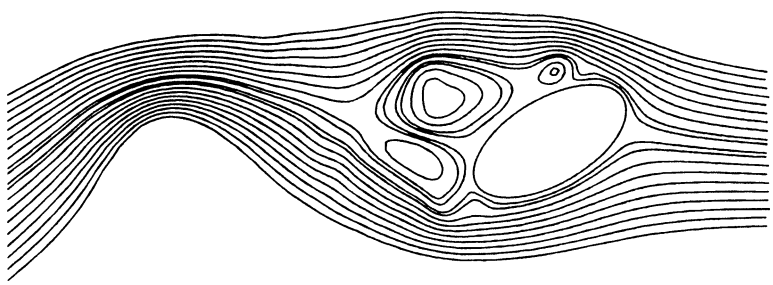

(d)

(*continued on next page*)

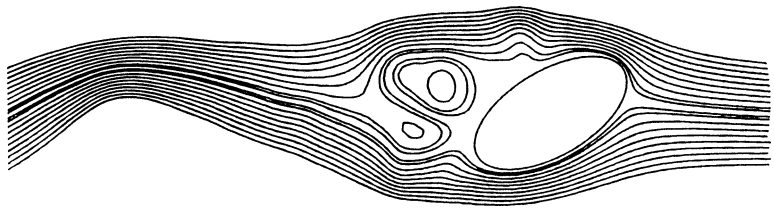

(e)

Fig. 2. Instantaneous streamlines of the flow for $R = 10^3$, $\Omega = \pi$, $r = 0.5$, $\eta = \pi/3$ and $\alpha = 0.5$: (a) $t = 10$, (b) $t = 10.5$, (c) $t = 11$, (d) $t = 11.5$, (e) $t = 12$.

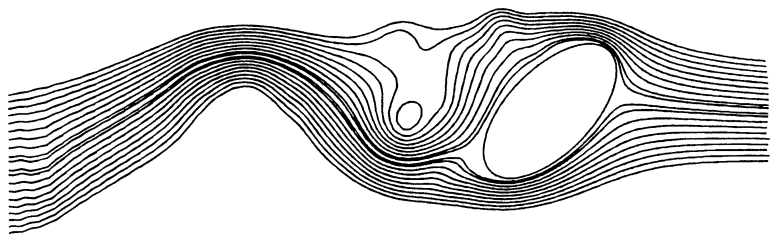

(a)

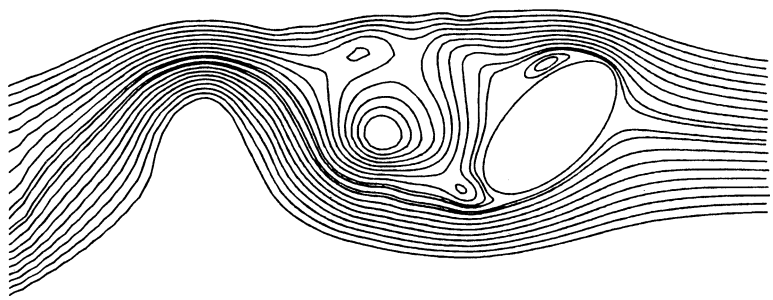

(b)

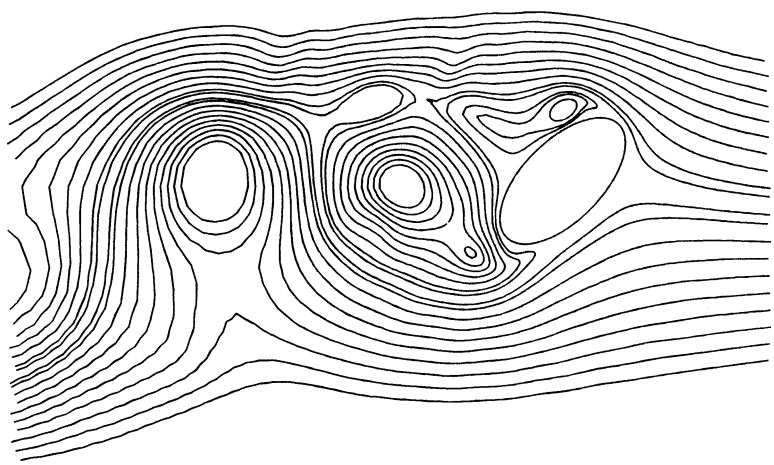

(c)

(*continued on next page*)

a two-in-one, coalescence between two vortices of like sign (double co-rotating vortex pair) in the lower half of the cylinder is also observed at $\tau = 11$. With the increase of time these double vortex pairs become weak and are convected downstream with the aid of the unidirectional cylinder motion. This continues until the end of the sixth complete oscillation, Fig. 2(e), when the oscillatory velocity is maximum. At even times the streamlines are closest together since the cylinder moves against the incoming flow thus increasing the relative velocity; at odd times the streamlines are furthest apart since the cylinder is moving

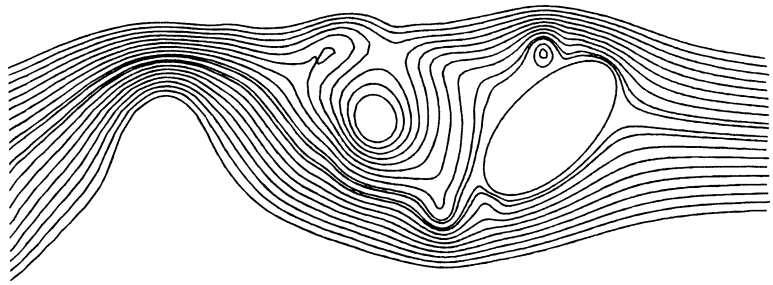

(d)

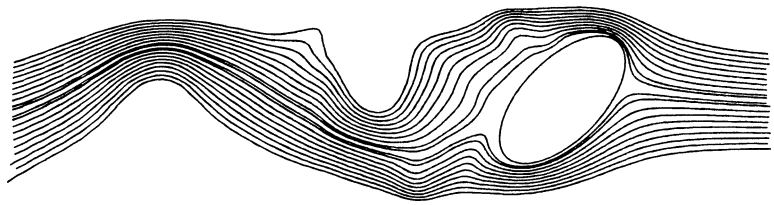

(e)

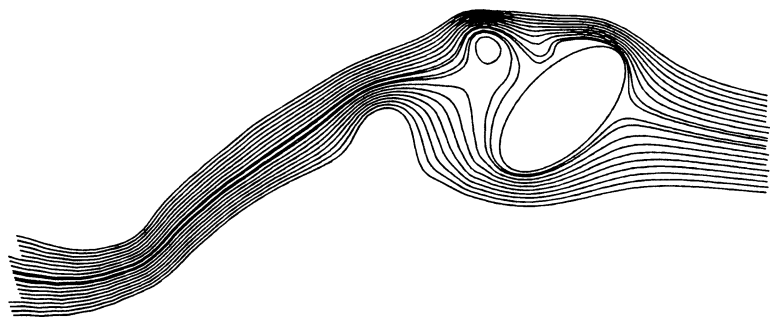

(f)

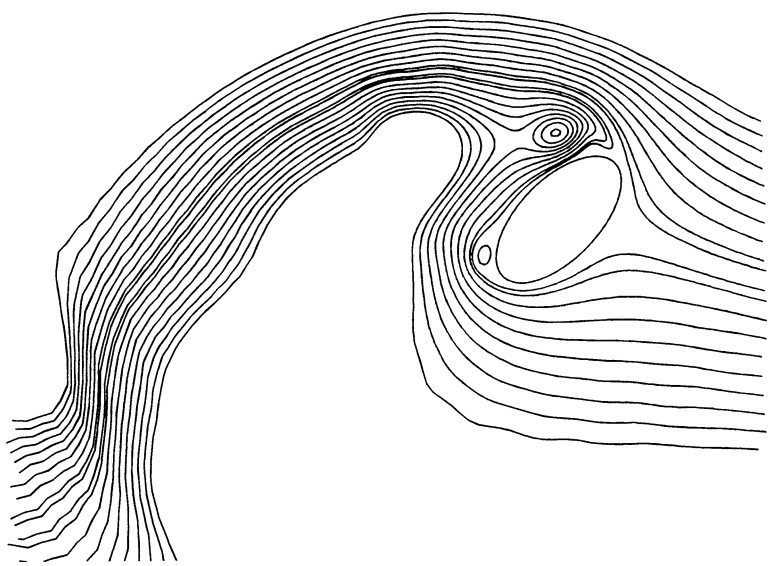

(g)

(*continued on next page*)

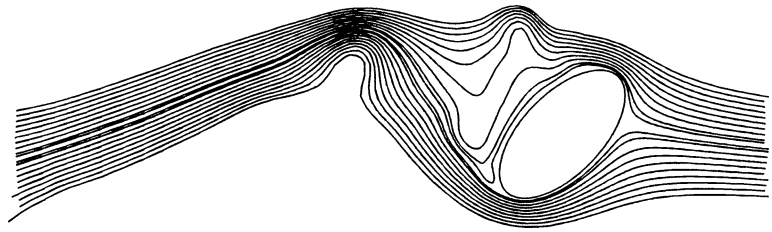

(h)

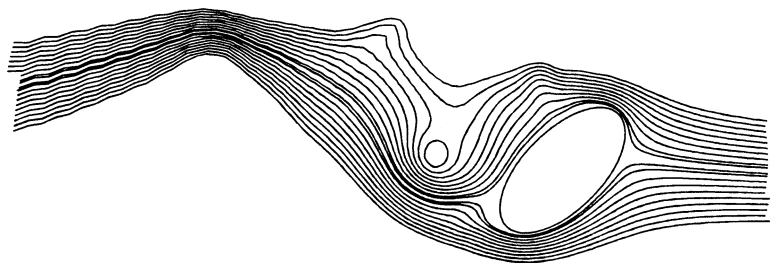

(i)

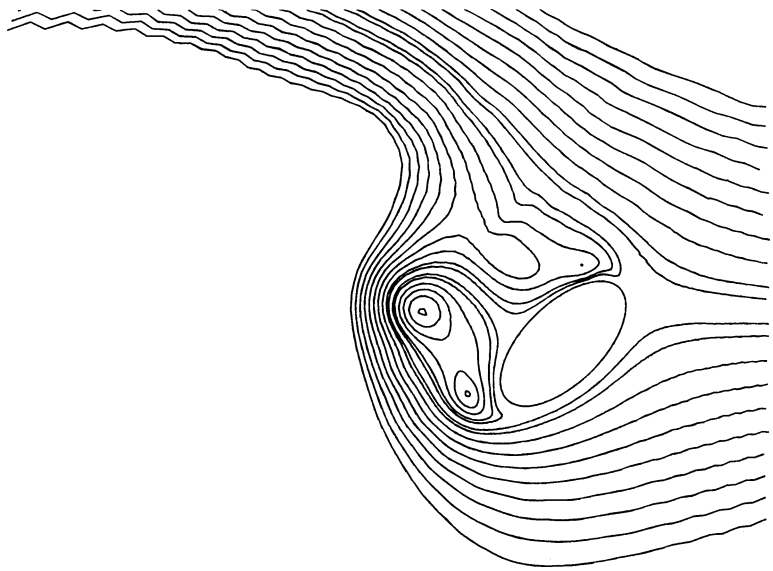

(j)

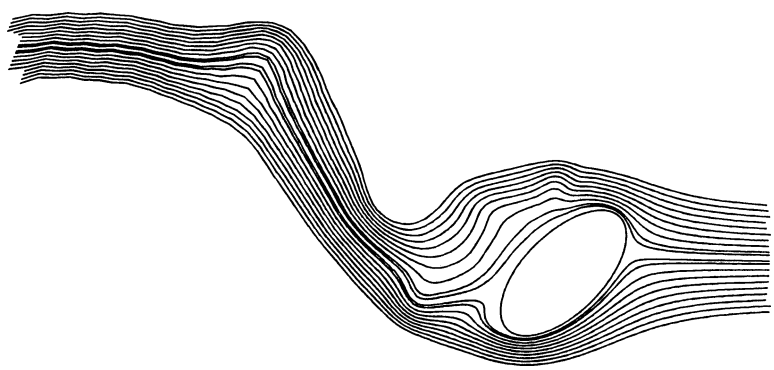

(k)

Fig. 3. Instantaneous streamlines of the flow for $R = 10^3$, $\Omega = \pi$, $r = 0.5$, $\eta = \pi/4$ and $\alpha = 0.5$: (a) $t = 10$, (b) $t = 10.5$, (c) $t = 11$, (d) $t = 11.5$, (e) $t = 12$, (f) $t = 18$, (g) $t = 19$, (h) $t = 20$, (i) $t = 22$, (j) $t = 23$, (k) $t = 24$.

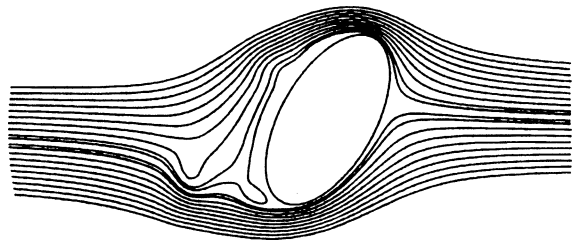

(a)

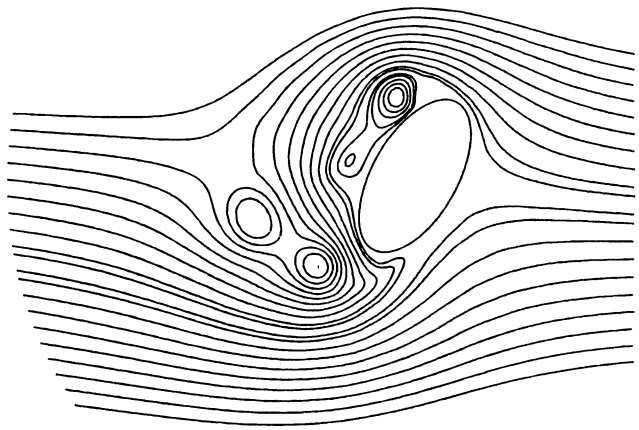

(b)

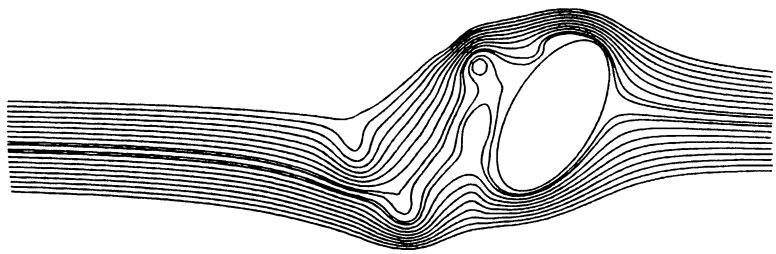

(c)

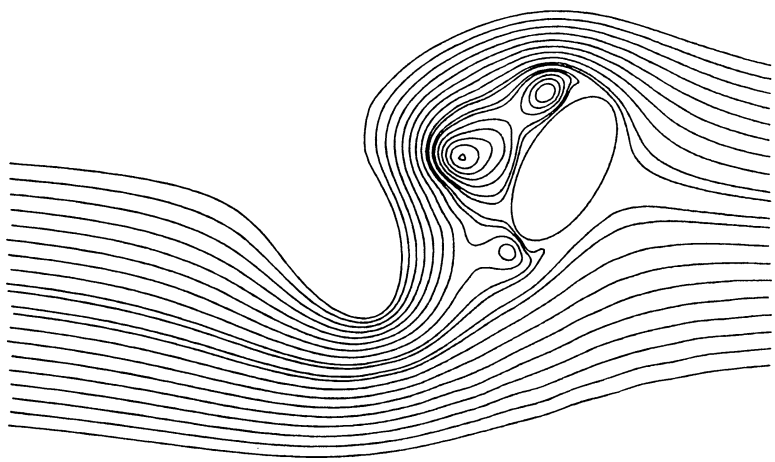

(d)

(*continued on next page*)

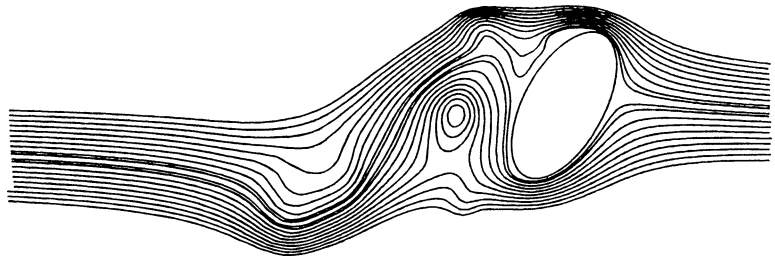

(e)

(f)

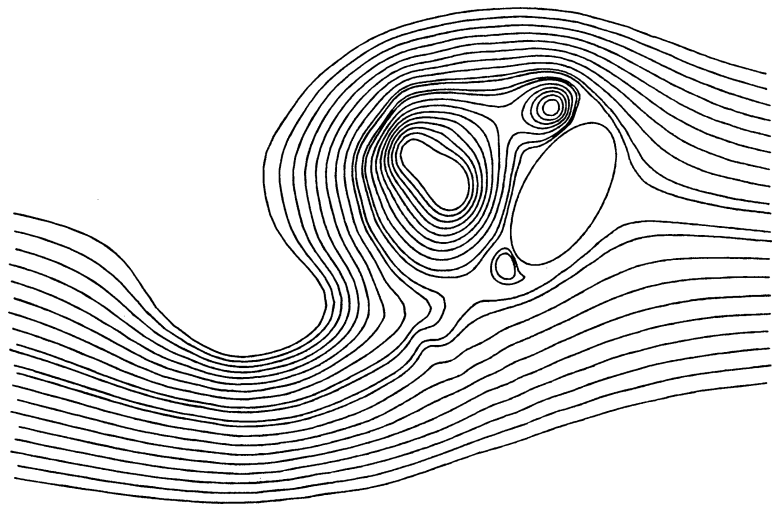

(g)

(h)

(*continued on next page*)

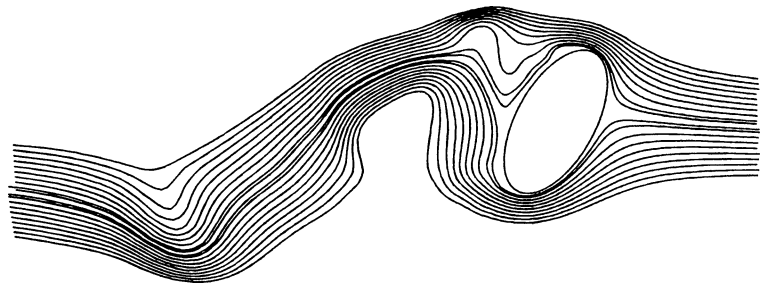

(i)

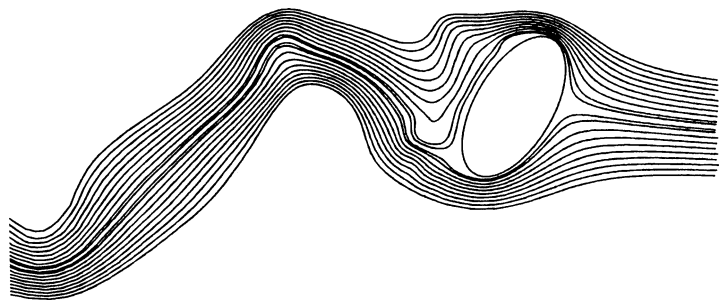

(j)

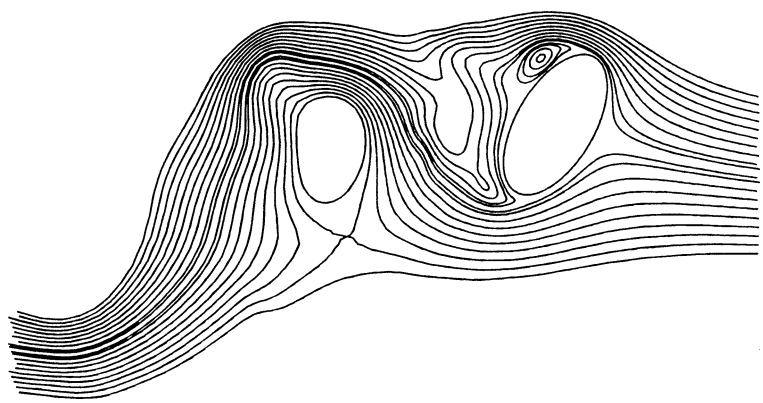

(k)

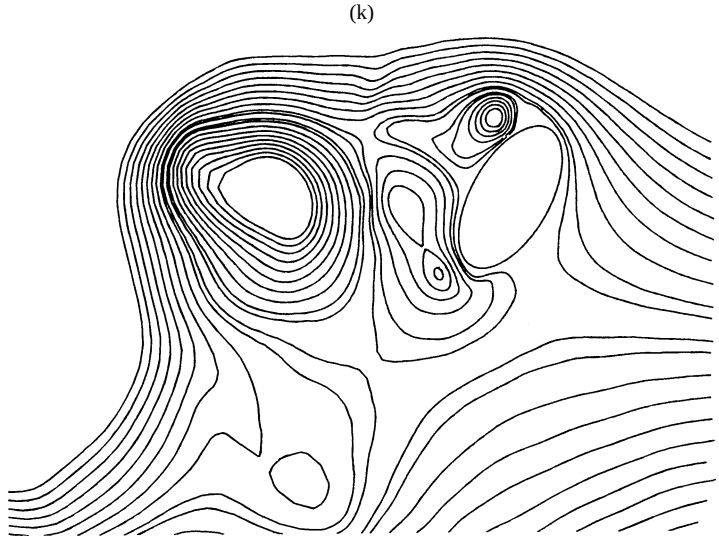

(l)

(*continued on next page*)

(m)

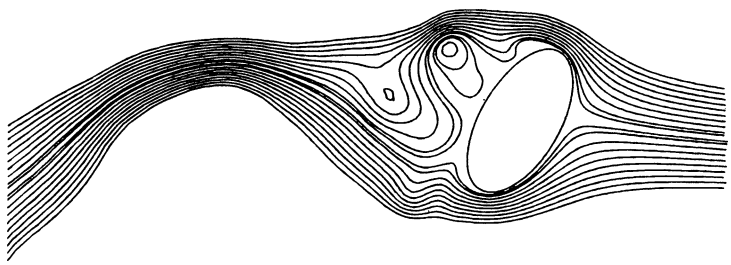

(n)

Fig. 4. Instantaneous streamlines of the flow for $R = 10^3$, $\Omega = \pi$, $r = 0.5$, $\eta = \pi/6$ and $\alpha = 0.5$: (a) $t = 2$, (b) $t = 3$, (c) $t = 4$, (d) $t = 5$, (e) $t = 6$, (f) $t = 6.5$, (g) $t = 7$, (h) $t = 7.5$, (i) $t = 8$, (j) $t = 10$, (k) $t = 10.5$, (l) $t = 11$, (m) $t = 11.5$, (n) $t = 12$.

in the same direction as the incoming flow thus reducing the relative velocity. At half times (i.e., $\tau = 10.5, 11.5$) the cylinder is momentarily at rest.

Shown in Fig. 3 are eleven snap shots of the flow for the case of $\eta = \pi/4$. In the near wake, vortex patterns are synchronized with the cylinder oscillation and they are similar to those for the smaller inclination angle ($\eta = \pi/6$) during the sixth cycle when $10.0 \leqslant \tau \leqslant 12.0$, showing periodic behaviour. Figs. 3(f)–(k) illustrate the flow at six instants in time during the tenth and twelfth cycles of oscillation for the time intervals $18.0 \leqslant \tau \leqslant 20.0$ and $22.0 \leqslant \tau \leqslant 24.0$, respectively. The vortices in the near wake are simply the result of one vortex in each half oscillation cycle. Also, a double co-rotating vortex pair is observed beyond the near-wake every other cycle (see for example Figs. 3(c)–(j) at $\tau = 11, 23$). In the near-wake, the vortex modes in the case of $\eta = \pi/4$ when $\alpha = 0.25, 0.75$ (not shown here) are similar to the case of $\alpha = 0.5$.

In Fig. 4 the angle of inclination is increased to $\eta = \pi/3$ and the instantaneous streamline patterns are plotted during the time interval $2.0 \leqslant \tau \leqslant 12.0$. It is found that the near-wake structure share many similarities with the other cases considered previously. During each cycle, two small-scale vortices of opposite sign are shed alternately from the upper and lower sides of the cylinder. Moreover, a two-in-one, coalescence between two vortices of like sign is observed beyond the near wake every cycle (see for example Figs. 4(b, d, g, l) at $\tau = 3, 5, 7, 11$).

Comparison of the Figs. 4(a)–(e) with the corresponding ones for the cases of $\eta = \pi/6, \pi/4$ indicates that, with the increase of η, the size of the separated flow region decreases whereas the vortex shedding process speeds up slightly. This increases the rate at which the flow reaches a periodic state. The only other point worth emphasizing is that the lateral spacing of the vortex street seems to be increasing as η increases from $\pi/6$ to $\pi/3$.

The time variation of the streamline patterns for the case $\eta = \pi/2$ is shown in Figs. 5(a)–(k) for selected values of τ between $\tau = 2$ and 12. Fig. 5(a) shows the streamlines when the oscillatory velocity is zero. This figure shows a pair of symmetric co-rotating vortices in the regions $90° \leqslant \theta \leqslant 180°$ and $180° \leqslant \theta \leqslant 270°$. After a while, this vortex pair detaches and moves downstream, initiating an alternate shedding process. It is noted that at $\tau = 4$ and 6.5 the two co-rotating vortex pairs are shed away to form adjacent vortices of the same sign. The interval between $\tau = 6$ and $\tau = 8$ represents the fourth complete oscillation cycle following the start of the motion. Figs. 5 (e), (g) and (i) represents the situation at the beginning, middle and end of the oscillation respectively. On the other hand, Figs. 5 (f) and (h) represent the times at which the oscillatory motion comes to a complete rest. At the end of the sixth cycle when $\tau = 12$ we once again observe shedding of a double co-rotating vortex pair in the cylinder wake and the movement of it in the downstream direction. For larger times Figs. 5(l)–(t) exhibit a single asymmetrical mode of vortex formation as expected: the streamline patterns show alternate shedding of vortices from either

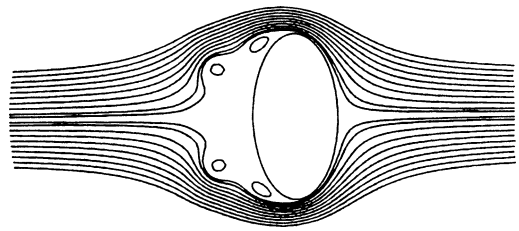

(a)

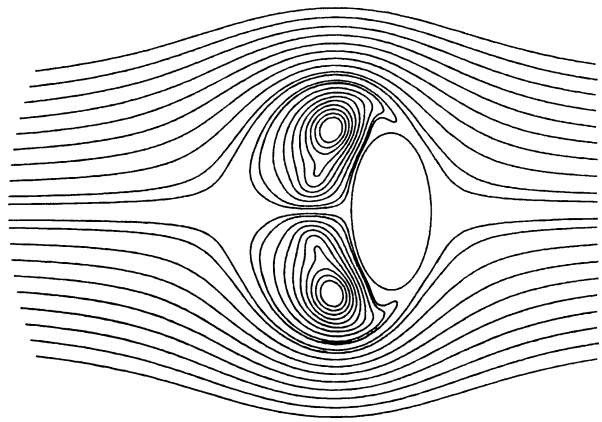

(b)

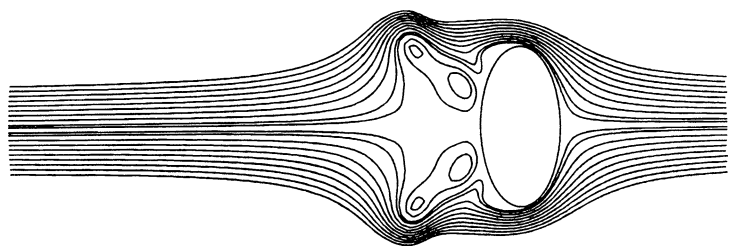

(c)

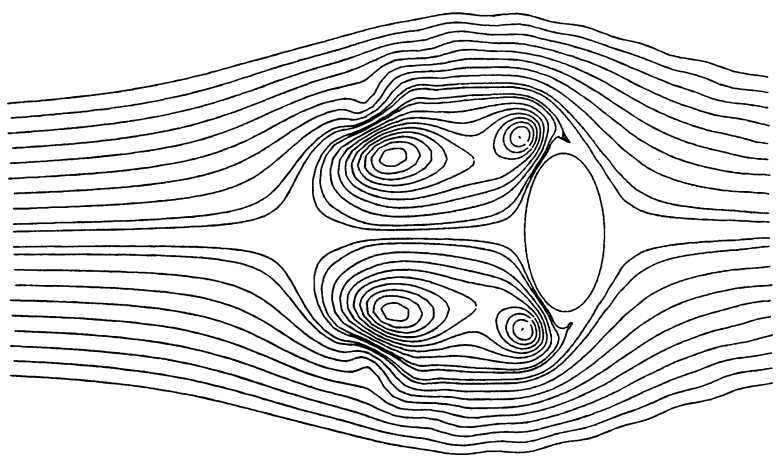

(d)

(*continued on next page*)

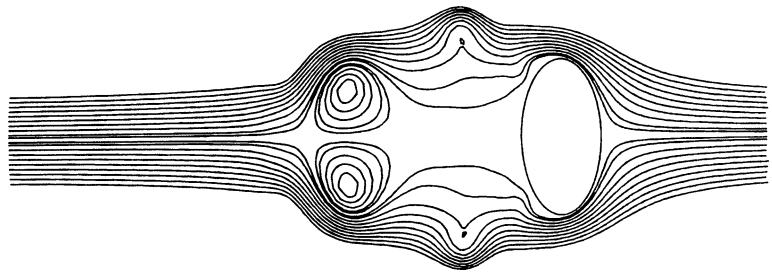

(e)

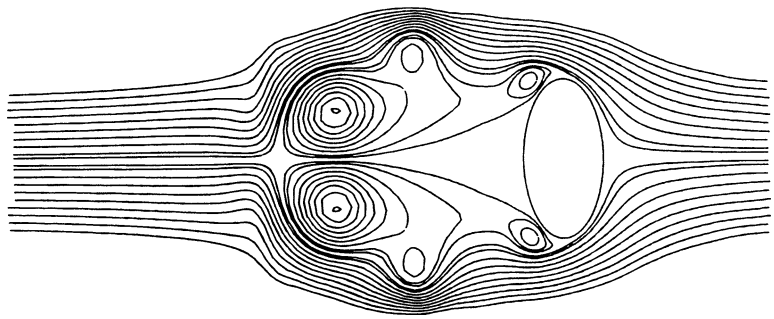

(f)

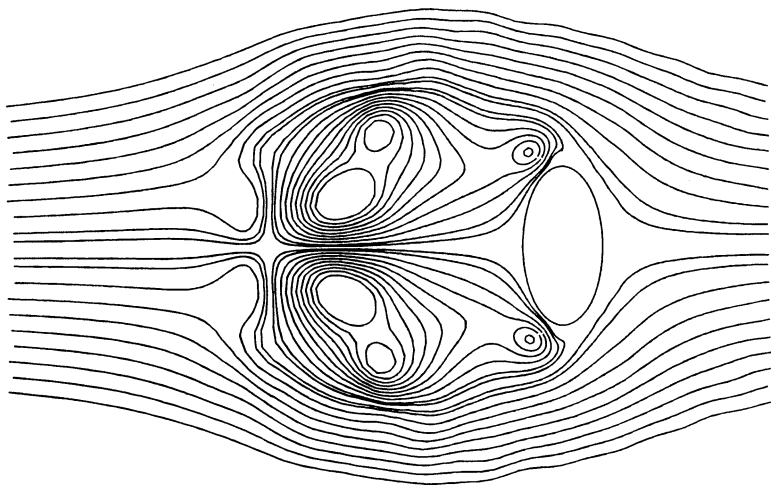

(g)

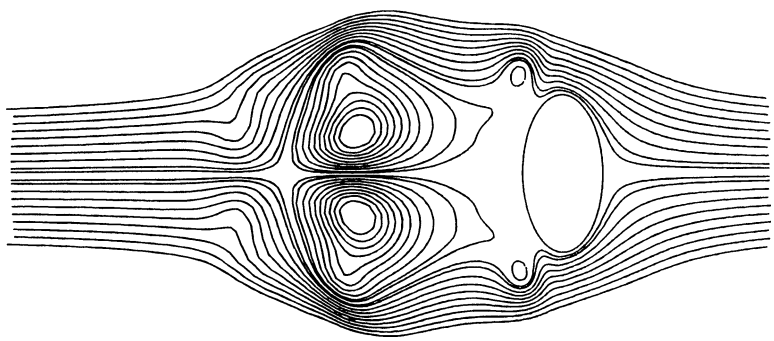

(h)

(*continued on next page*)

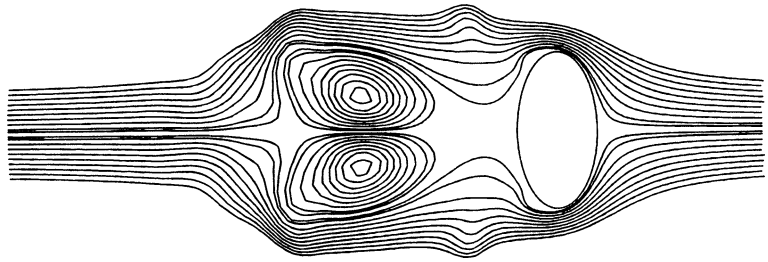

(i)

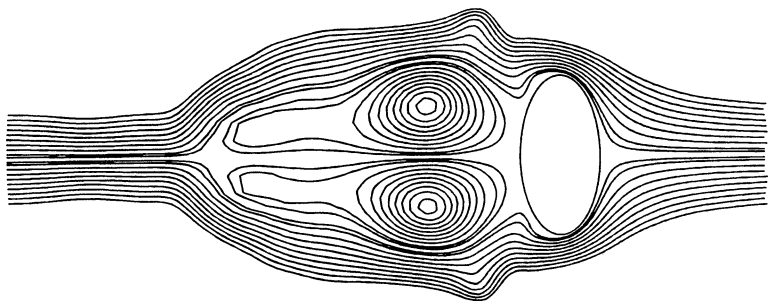

(j)

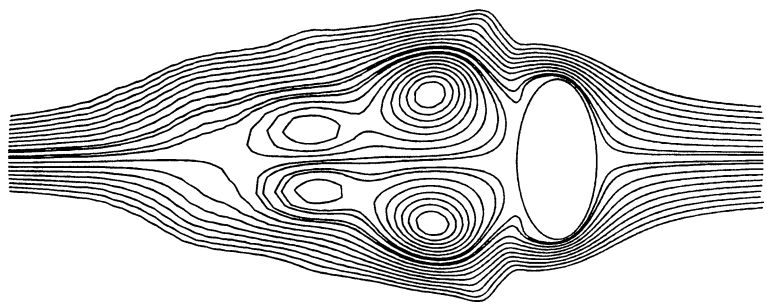

(k)

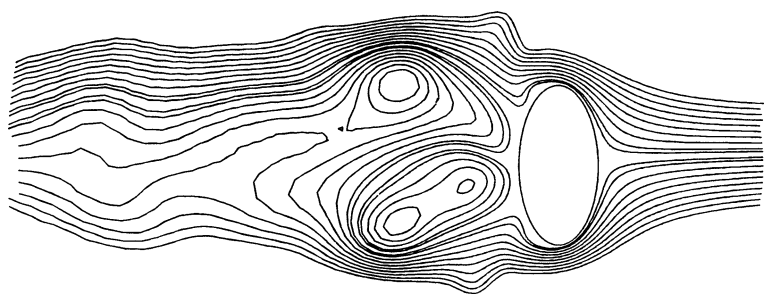

(l)

(*continued on next page*)

side of the cylinder over an oscillation cycle; this is the classical mode of vortex shedding leading to formation of the Kármán street. This asymmetry first becomes apparent at $\tau = 12$. During the time interval $14 \leqslant t \leqslant 24$ for odd times ($\tau = 15, 17$) the streamlines are spaced much further apart than for even times ($\tau = 14, 16, 18, 20, 22, 24$). This is because of the increase in velocity relative to the cylinder due to the inline oscillations. Also, the periodic nature of the flow field in the near wake begins to develop after the tenth cycle of oscillation: Figs. 5 (s) and 5 (t) are almost the same, showing the repetitive nature of the flow field at $\tau = 22$ and $\tau = 24$. Small deviations between these streamline patterns are due to the fact that numerical solution was not advanced far in time to achieve an exact periodic flow field.

Comparison of these figures with the corresponding ones in the cases of $\eta = \pi/6, \pi/4, \pi/3$ indicates that although the vortices are the result of single vortex shedding in each half cycle of the oscillation; the near-wake structure is drastically

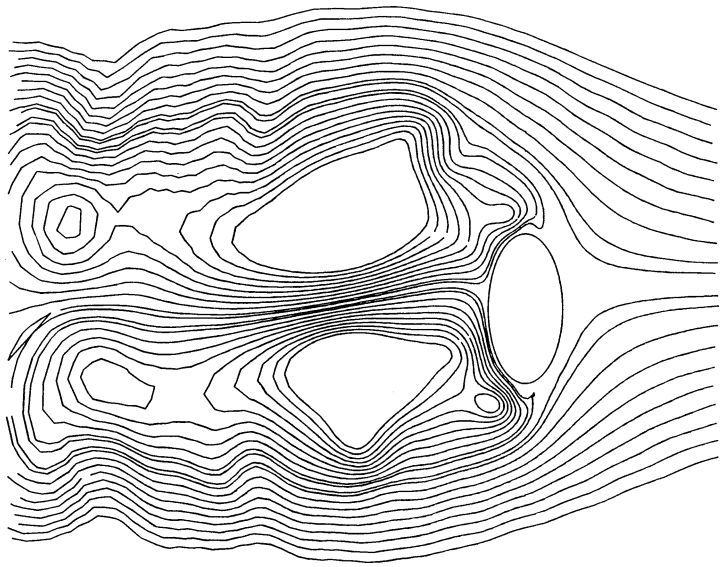

(m)

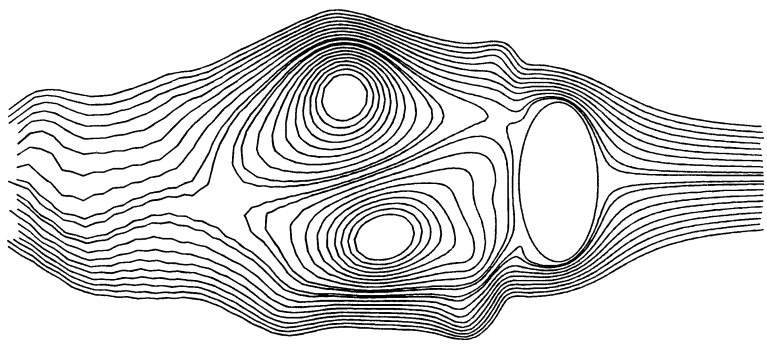

(n)

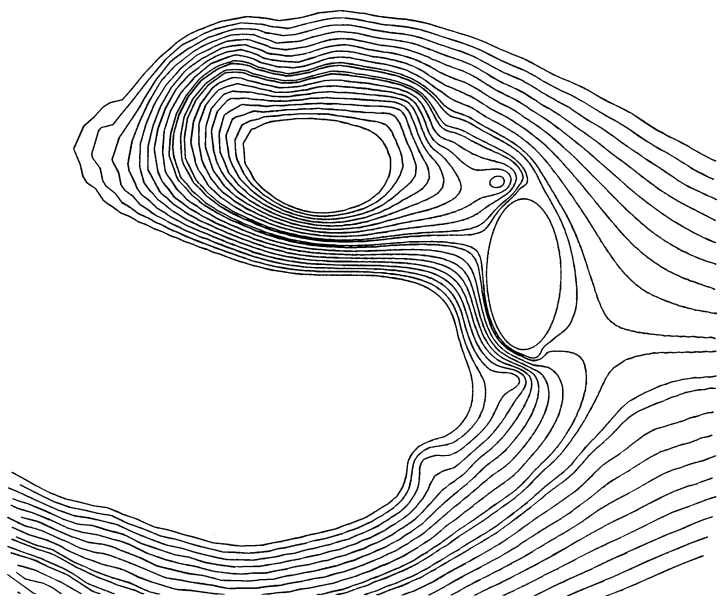

(o)

(*continued on next page*)

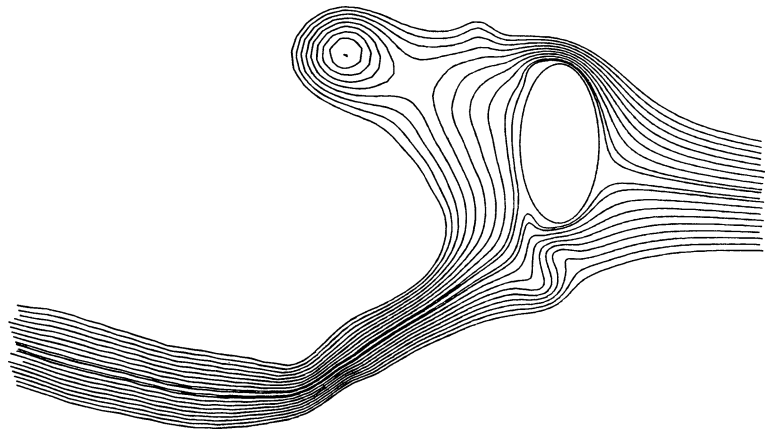

(p)

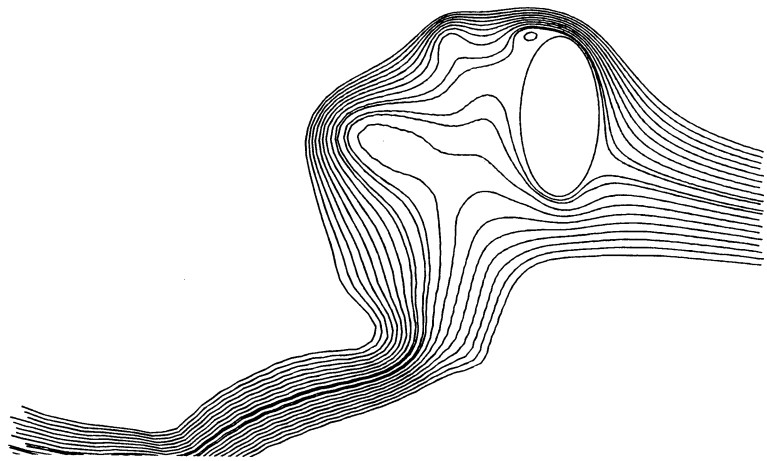

(r)

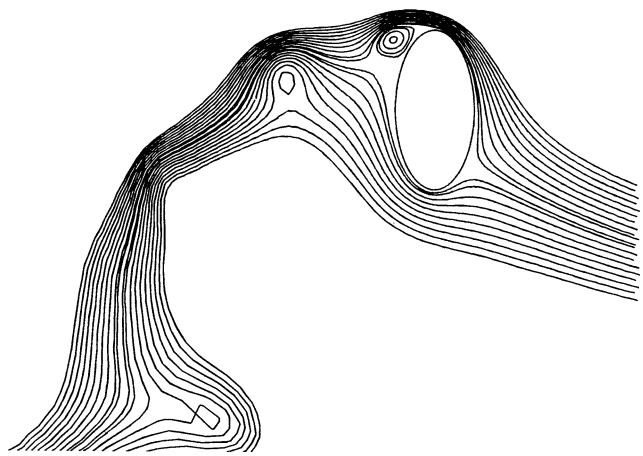

(s)

(*continued on next page*)

different from the ones obtained in the case of $\eta = \pi/2$. Two distinct forms of vortex street were observed when the inclined elliptic cylinder was vibrated in-line with the flow. First of these, when $0 < \eta < \pi/2$, is characterized by the shedding of two vortices of opposing sign during each cycle of the cylinder's motion. The resulting pattern has vortices of like sign, but the near-wake can be characterized generally as an alternating street of vortex pairs with each pair made up of two vortices of opposing

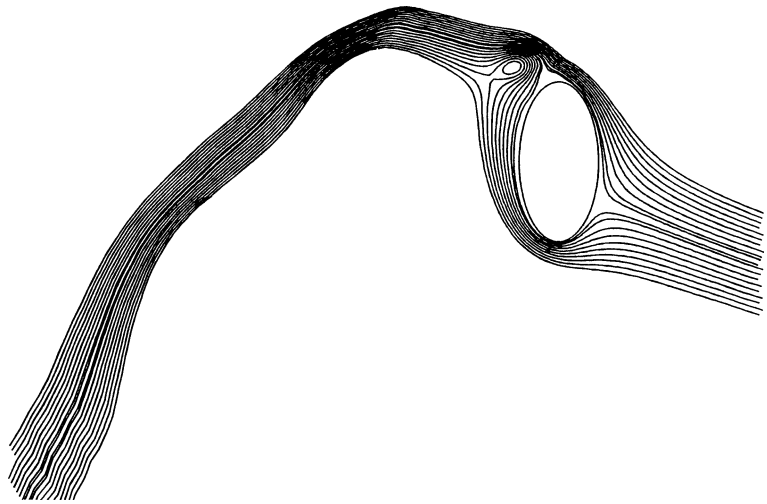

(t)

Fig. 5. Instantaneous streamlines of the flow for $R = 10^3$, $\Omega = \pi$, $r = 0.5$, $\eta = \pi/2$ and $\alpha = 0.5$: (a) $t = 2$, (b) $t = 3$, (c) $t = 4$, (d) $t = 5$, (e) $t = 6$, (f) $t = 6.5$, (g) $t = 7$, (h) $t = 7.5$, (i) $t = 8$, (j) $t = 10$, (k) $t = 12$, (l) $t = 14$, (m) $t = 15$, (n) $t = 16$, (o) $t = 17$, (p) $t = 18$, (r) $t = 20$, (s) $t = 22$, (t) $t = 24$.

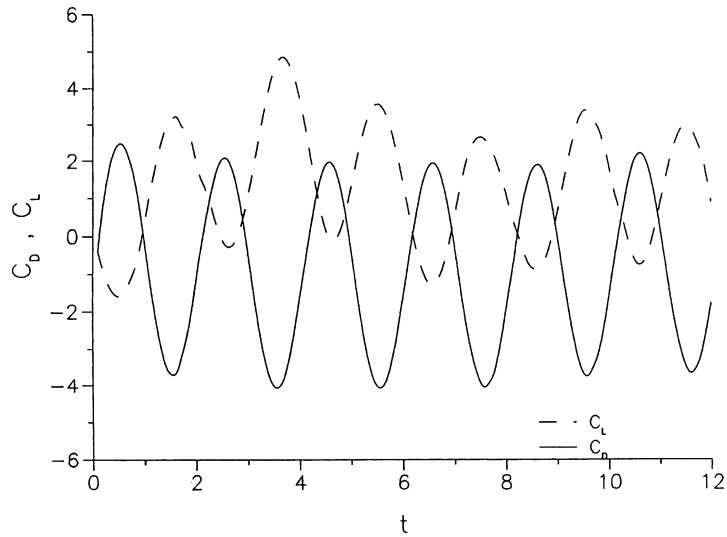

Fig. 6. Variation of the total drag and lift coefficients, (a) C_D and (b) C_L, with τ at $R = 10^3$, $\Omega = \pi$, $r = 0.5$, $\eta = \pi/6$: $\alpha = 0.5$.

rotation. The second form of street, when $\eta = \pi/2$, is characterized by the shedding of unusual two vortex pairs during each cycle of the motion. The resulting pattern is very complex and each pair involves vortices of like sign in the near-wake region.

4.2. Force coefficients for $R = 10^3$, $\Omega = \pi$ and $r = 0.5$ when $0.25 \leqslant \alpha \leqslant 0.75$

To discuss the effects of the angle of inclination and the velocity ratio on the force coefficients results are presented in Figs. 6–9 for the cases of $\eta = \pi/6, \pi/4, \pi/3, \pi/2$ when $0.25 \leqslant \alpha \leqslant 0.75$. These figures indicate the periodic variation of the flow field associated with vortex shedding. For all cases, both lift and drag coefficients vary at the cylinder frequency and they are out-of-phase with each other. It is noted that maximum values for C_L are attained near the equilibrium position of the cylinder during the unidirectional motion of the cylinder in the horizontal direction.

Fig. 7 shows the variations of drag and lift coefficients for the case of $\eta = \pi/4$ when $\alpha = 0.25, 0.5, 0.75$. The amplitude of oscillation of both C_D and C_L tend to be larger as the velocity ratio increases. The maximum values of C_D for each value of α are in phase with each other.

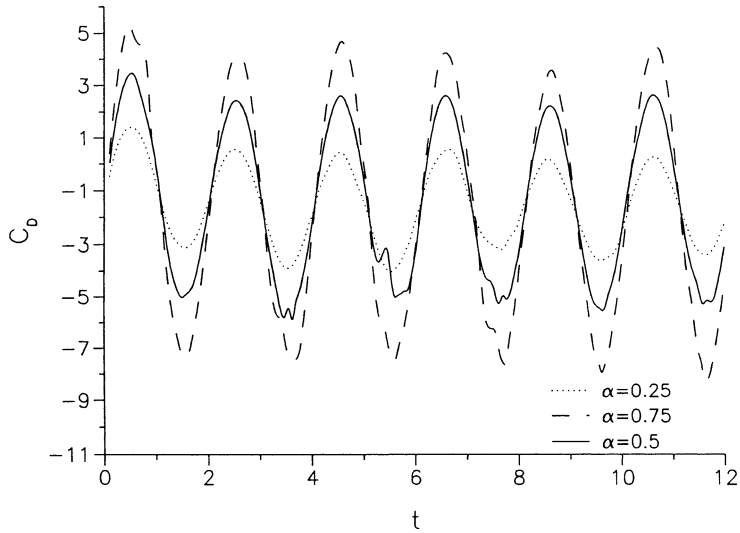

(a)

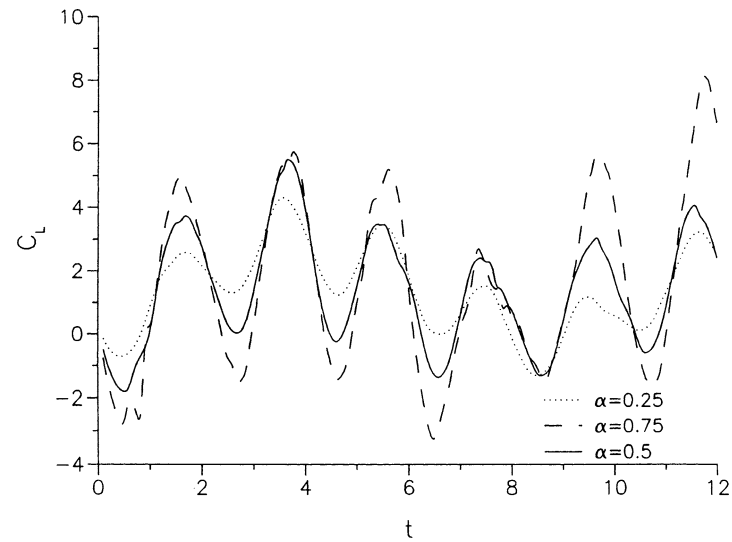

(b)

Fig. 7. Variation of the total drag and lift coefficients, (a) C_D and (b) C_L, with τ at $R = 10^3$, $\Omega = \pi$, $r = 0.5$, $\eta = \pi/4$: $\alpha = 0.25, 0.5, 0.75$.

Fig. 9 shows the time variation of the drag coefficient for the case of $\eta = \pi/2$ when $\alpha = 0.25,\ 0.5$. Here, the drag coefficient varies at the cylinder oscillation frequency. It can be also seen that the increase of the velocity ratio makes the amplitude of the fluctuating drag force, C_D, slightly larger.

5. Conclusions

The present paper summarizes results of numerical flow investigations with flow being induced by an inclined elliptic cylinder which is subject to harmonic rectilinear oscillations in-line with the flow. The effects of the angle of inclination and velocity ratio are discussed. The cases of $\eta = \pi/6, \pi/4, \pi/3, \pi/2$ are calculated in a range of velocity ratio $0.25 \leqslant \alpha \leqslant 0.75$ at the Reynolds number of $R = 10^3$ and the forcing Strouhal number $\Omega = \pi$ when $r = 0.5$. Two distinct forms of vortex street were observed depending on the values of the angle of inclination. In all the cases considered in this study, a two-in-one, coalescence between two vortices of like sign (double co-rotating vortex pair) is observed on one side of the cylinder. Drag

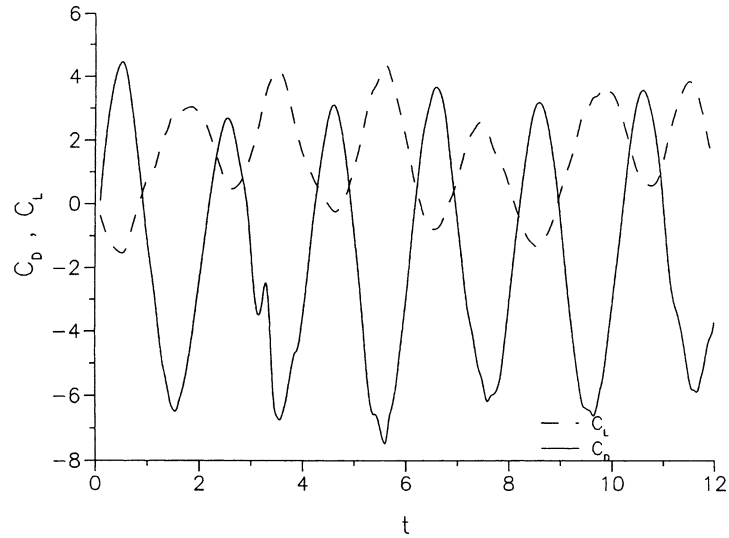

Fig. 8. Variation of the total drag coefficient, C_D with τ at $R = 10^3$, $\Omega = \pi$, $r = 0.5$, $\eta = \pi/3$: $\alpha = 0.5$.

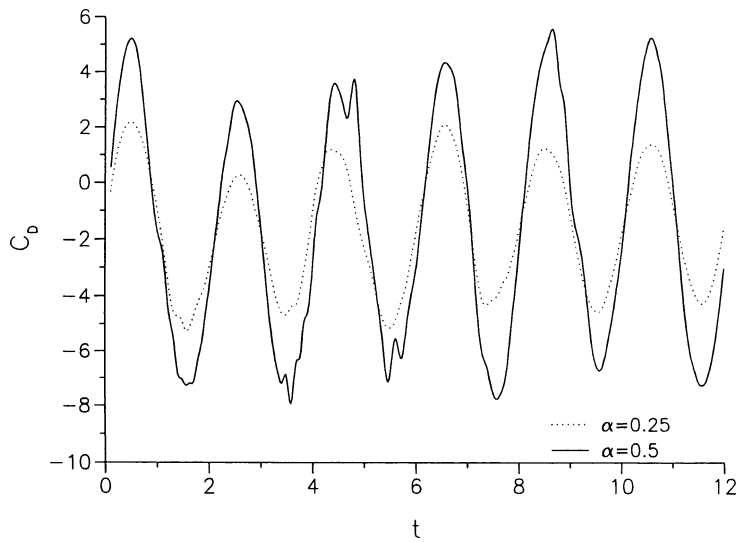

Fig. 9. Variation of the total drag coefficient, C_D with τ at $R = 10^3$, $\Omega = \pi$, $r = 0.5$, $\eta = \pi/2$: $\alpha = 0.25, 0.5$.

and lift forces are extracted from the computations and shown to be dependent upon forced oscillation amplitude and angle of inclination. They oscillate with the forcing frequency of the cylinder.

A word of explanation is needed regarding the applicability of two-dimensional results. Although physically the wake may be three-dimensional, we believe that it can be represented reasonably well by a two-dimensional model in the near-wake region which this study focuses on. On the evidence that spanwise correlations of forces, wake vortices, etc. all increase with transverse cylinder vibration at a frequency at or near the vortex shedding (e.g., Ramberg and Griffin [14] and Blackburn and Henderson [15]) it is reasonable to suggest that harmonic motion of a long cylinder seems to suppress the three-dimensionality and produce flows that are more two-dimensional than their fixed-cylinder counterparts, at least in the near wake region.

Acknowledgements

The support of the Natural Sciences and Engineering Council of Canada is gratefully acknowledged.

References

[1] N. Riley, Oscillatory viscous flows. Review and extension, J. Inst. Math. Appl. 3 (1967) 419–436.
[2] T. Sarpkaya, Vortex-induced oscillations. A selective review, J. Appl. Mech. 46 (1979) 241–256.
[3] B.M. Sumer, J. Fredsøe, Hydrodynamics Around Cylindrical Structures, World Scientific, 1997.
[4] A. Okajima, H. Takata, T. Asanuma, Viscous flow around a transversally oscillating elliptic cylinder, Inst. Space and Aero. Sci. (Univ. Tokyo), Rep. 533, 1975.
[5] S.J.D. D'Alessio, S. Kocabiyik, Numerical simulation of the flow induced by a transversely oscillating inclined elliptic cylinder, J. Fluids Struct. 15 (2001) 691–715.
[6] B.J. Davidson, N. Riley, Jets induced by oscillatory motion, J. Fluid Mech. 53 (1972) 287–303.
[7] S. Taneda, Visual study of unsteady separated flows around bodies, Prog. Aerospace Sci. 17 (1977) 287–348.
[8] P. Hall, On the stability of the unsteady boundary layer on a cylinder oscillating transversely in a viscous fluid, J. Fluid Mech. 146 (1984) 347–367.
[9] H.M. Badr, S. Kocabiyik, Symmetrically oscillating viscous flow over an elliptic cylinder, J. Fluids Struct. 11 (1997) 745–766.
[10] A.N. Staniforth, Ph.D. Thesis, University of Western Ontario, London, Ontario, Canada, 1972.
[11] S.J.D. D'Alessio, S.C.R. Dennis, P. Nguyen, Unsteady viscous flow past an impulsively started oscillating and translating elliptic cylinder, J. Engrg. Math. 35 (1999) 339–357.
[12] S.C.R. Dennis, L. Quartapelle, Some uses of Green's Theorem in solving the Navier–Stokes equations, Int. J. Numer. Methods Fluids 9 (1989) 871–890.
[13] S.C.R. Dennis, G.-Z. Chang, Numerical integration of the Navier–Stokes equations in two-dimensions, Mathematics Research Center, University of Wisconsin, Technical Summary Report No. 859, 1969.
[14] S.E. Ramberg, O.M. Griffin, Velocity correlation and vortex spacing in the wake of a vibrating cable, ASME J. Fluids Engrg. 98 (1976) 10–18.
[15] B.M. Blackburn, R.D. Henderson, A study of two-dimensional flow past an oscillating cylinder, J. Fluid Mech. 385 (1999) 255–286.